CONCRETE RESEARCH LETTERS
www.crl.issres.net
Vol. 4 (4) – Dec. 2013

Strengthening of Concrete Beams in Shear

Medhat Mohammed[a], Ahmed A Elshafey[a,*], Mostafa M. El-Shami[b], and Kamel S Kandil[a]

[a]*Department of Civil Engineering, Faculty of Engineering, Menoufyia University, Shebin El-Kom, Menoufyia, Egypt.*
[b]*Construction Eng. Dept., University of Dammam, Kingdom of Saudi Arabia.*

Received: 10/09/2013 – Revised 25/10/2013 – Accepted 15/11/2013

Abstract

Finite element analysis (FEA) is used to predict the behavior of reinforced concrete beams strengthened in shear with fiber reinforced polymer (FRP). To verify and measure the accuracy of the FEM model, the FEA results were compared with both pervious experimental and theoretical results. Two beams were studied simulating the Horsetail Creek Bridge in Oregon, USA. The first one is a control beam with no strengthening fiber. The second one is wrapped with glass fiber reinforced polymer (GFRP) laminates to reinforce the beam in shear. Results were represented by load-strain curves for concrete, steel and fiber. In addition, the load deflection curves and crack patterns developed in the beams were presented. The results showed that FE modeling was accurate in simulating the tested beams. It was also clear that using FRP in strengthening reinforced concrete beams is an effective method in improving shear behavior of the beams.

Keywords: GFRP; Finite element; Shear strengthening; Concrete; Beam.

1. Introduction

Strengthening and repairing of concrete elements is widely used worldwide as the structures deteriorate with time. Some parameters control the use of strengthening technique such as cost and time. Currently, strengthening with FRP is the most common technique used these days. In the past, concrete elements were strengthened by using additional beams, props, or external post-tensioning. However, advances in technology led to the invention of plate bonding technique. Since 1960 retrofitting using steel plates was used around tension face of the elements by using a suitable adhesive. In 1980, FRP proved to be advantageous over steel plates in strengthening several reasons such as its light weight, resistance to corrosion, high strength and stiffness [1].

Various studies have been done on FRP strengthening of concrete elements. Different types of fibers were used such as CFRP, GFRP and aramid fiber reinforced polymer (AFRP) for repair in shear [2]. Several researchers investigated the effect of environmental condition, such as freeze /thaw or wet/dry cycling in a calcium chloride solution [3]. Preparation type and effect of resin type were studied by [4, 5]. Experimental tests were done as well as an analytical models based on finite element method (FEM) [6-8]. Also, the effect of loading technique (normal loading or cyclic loading) was studied [4]. Most expected failure modes that can occur were also investigated [9-11].

The objectives of this research is to investigate the effect of FRP shear strengthening of reinforced concrete beams using Finite Element Method (FEM), compare the analytical model results with the experimental results from previous studies to accurately calibrate the model, and study the effect of using GFRP sheets on shear strengthening of reinforced concrete beams. An

efficient finite element model is introduced through this work. The finite element model was able to solve the beam model in a short time compared to any other previous models.

2. Finite element model

2.1 Geometry of studied beams

Full scale beams were studied with dimension of. The span between the two supports was. The distance between the two loads lines was as shown in Figure 1. Due to symmetry, one quarter of the full beam was modeled in the FE analysis. It should be noted that these dimensions were chosen to simulate the experimental and theoretical examples [2, 12]. Steel reinforcement details for the full-size beams are illustrated in Figure 2. The inclined portions of the steel bars existing in the tested beams were ignored in the FEM for simplicity.

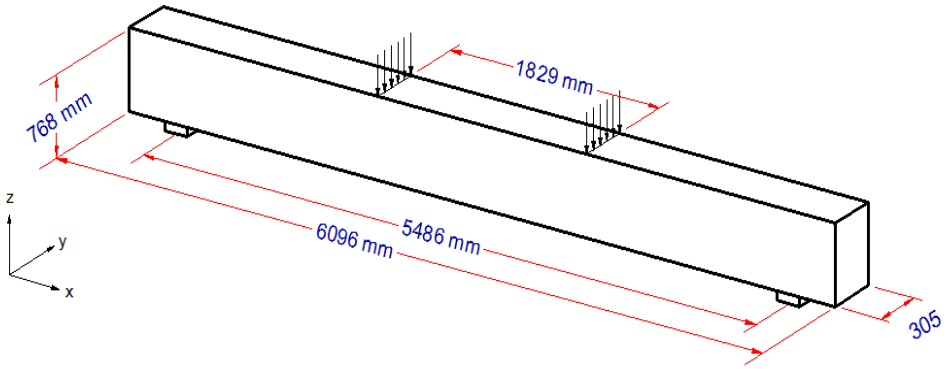

Figure 1: Typical beam dimensions.

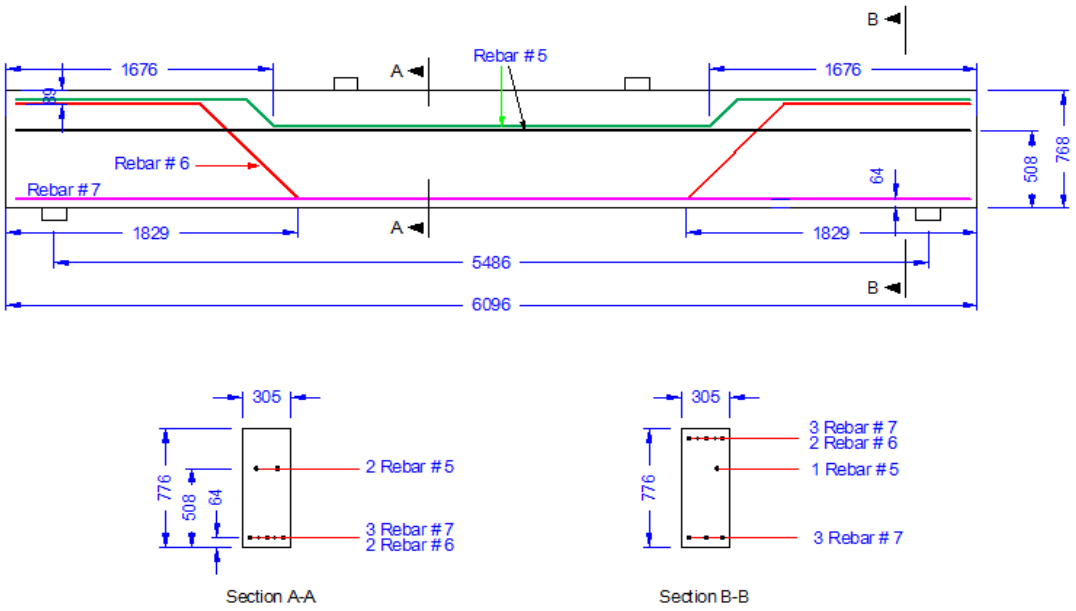

Figure 2: Typical steel reinforcement locations [2].

2.2 Finite element modelling (FEM)

Due to symmetry, a quarter of the full beam was modeled. The model is long, with a cross-section of only one loading plate and one support plate are modeled. In the experiment work, loading and support dimensions were approximately and; respectively. Beams reinforced by GFRP and CFRP composites have various thicknesses, depending upon the capacities needed at the various locations on the beams. The use of fibers with various thicknesses creates discontinuities, which are not desirable in the FE analysis. To overcome this problem, a constant overall thickness of FRP composite was used in the models. To keep the model equivalent, overall stiffness of the FRP materials, the elastic and shear modulus assigned to each FRP layer are modified to achieve the overall stiffness such as:

$$G_{xy} = \frac{E_x E_y}{E_x + E_y + 2\upsilon_{xy} E_X} \tag{1}$$

where,

is the shear modulus in the plane,
is the elastic modulus in the *x*-direction,
is the elastic modulus in the *y*-direction, and
is poison's ratio in the plane.

In FE analysis, some modifications of dimensions were done due to geometry, element connectivity, meshing of concrete and steel locations. Figure 3 shows the modified dimensions of the FRP reinforcing schemes for the quarter beam models.

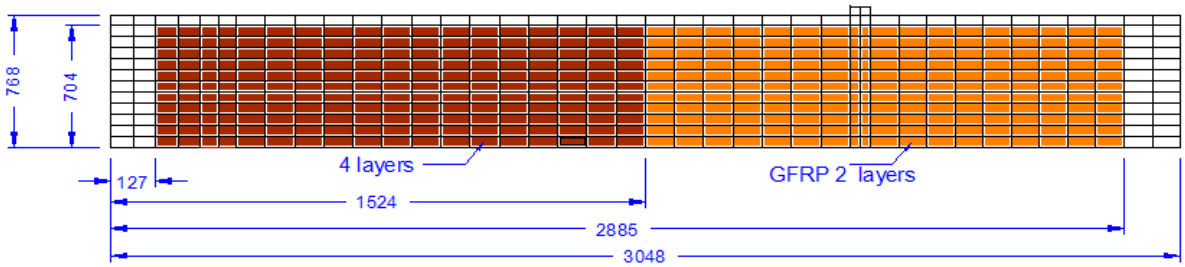

Figure 3: Modified dimensions of FRP reinforcing for strengthened shear beam.

2.3 Types of elements used in modeling

ANSYS, 2007 includes many elements which differ in properties, geometry, and degrees of freedom. The elements used in this research are:

- Solid element, SOLID65, was used for the concrete.
- Solid element, SOLID45, was used for steel plates at supports and loading area.
- Link element, LINK8, was used for steel rebars.
- Shell element, SHELL41, was used for FRP sheets.

2.4 Reinforced concrete

SOLID 65 was used for modeling concrete elements. SOLID 65 is capable of cracking in tension and crushing in compression. The eight-node element has three degrees of freedom at each node. The degrees of freedom are translations in the nodal *x*, *y*, and *z* directions. The most important aspect for this element is the treatment of nonlinear material properties. The concrete is capable of cracking (in three orthogonal directions), crushing, plastic deformation, and creep. SOLID 65 element is shown in Figure 4.

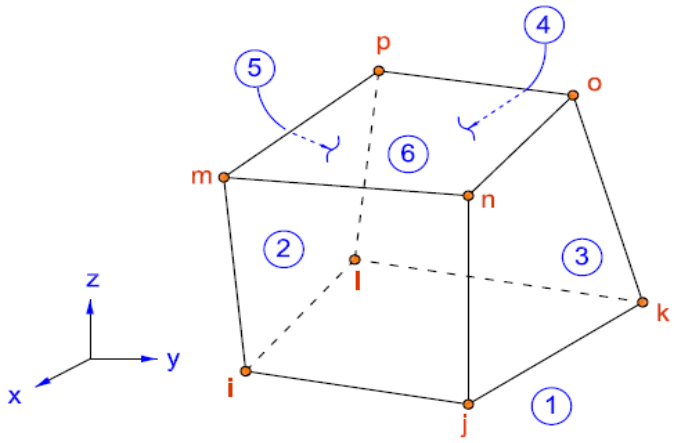

Figure 4: Solid 65 3-D reinforced concrete solid element.

2.5 Steel rebar

The 3-D spar element LINK8 was used to model the steel reinforcement. LINK8 is a two-node element having three degrees of freedom at each node; translations in the nodal *x*, *y*, and *z* directions. The element is also capable of plastic deformation, creep, swelling, stress stiffening, and large deflection capabilities. Figure 5 illustrates the geometry and node locations for this element type.

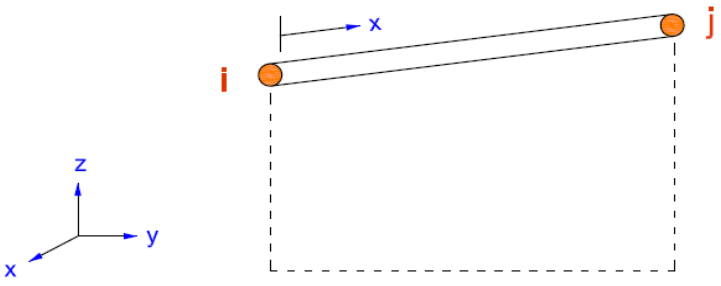

Figure 5: LINK8 3-D spar.

2.6 FRP composites

SHELL 41 element was employed to model the FRP composites; it is a 3-D element having membrane (in-plane) stiffness but no bending (out-of-plane) stiffness. It is intended for shell structures where bending of the elements is of secondary importance. The element has three degrees

of freedom at each node; translations in the nodal *x*, *y*, and *z* directions. The geometry, node locations, and the coordinate system are shown in Figure 6.

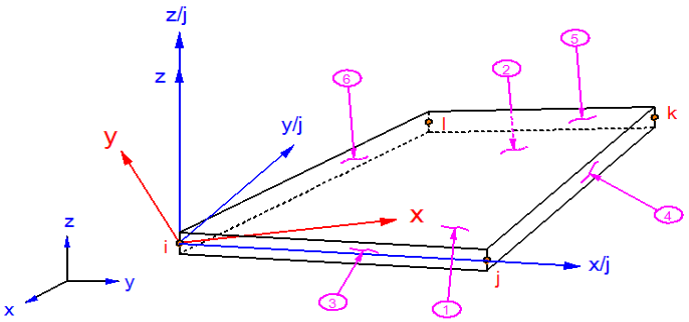

Figure 6: SHELL41 geometry and coordinate system.

2.7 Bond between elements

Perfect bond between elements was assumed. The link element for the steel reinforcing (LINK8) was connected between nodes of each adjacent concrete solid element (SOLID 65). The same approach was adopted for FRP composites as shown in Figure 7. The perfect bond assumption can be achieved using the high strength of the epoxy or by mechanical anchors used to attach FRP sheets to the experimental beams.

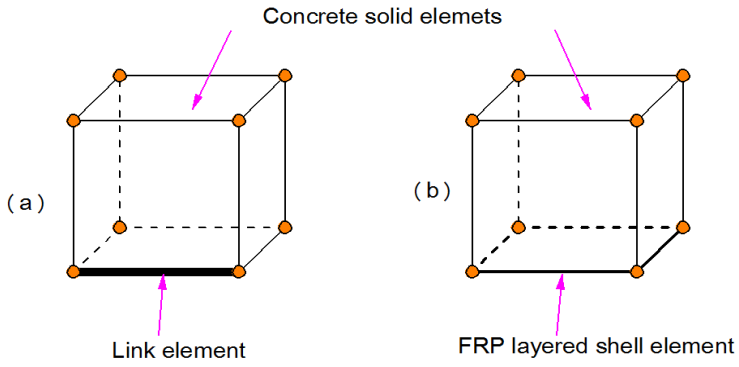

Figure 7: Element connectivity: (a) concrete solid element and link element
(b) Concrete solid element and FRP layered shell elements.

2.8 Supports and loading steel plates

SOLID 45 element was chosen to model steel plates at the supports and load application on the beam. The element is defined by eight nodes having three degrees of freedom at each node; translations in the nodal *x*, *y*, and *z* directions. The element has plasticity, creep, stress stiffening, large deflection, and large strain capabilities. The nodes location, geometry, and coordinate system are shown in Figure 8.

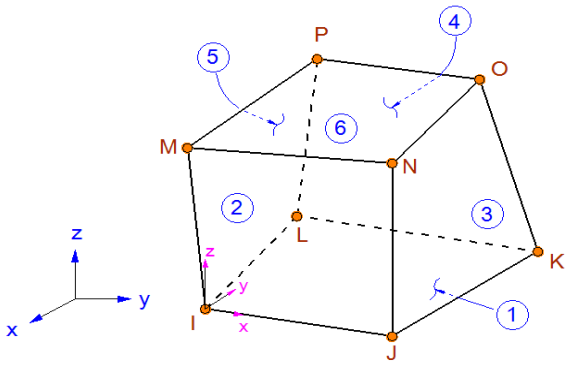

Figure 8: SOLID 45 3-D solid element (ANSYS, 2007).

3. Material properties

3.1 Concrete

Implementation of concrete properties in the model is a challenging task. Concrete has different behavior in tension and compression. Properties of concrete elements are shown in Table 1.

Table 1: SUMMARY OF MATERIAL PROPERTIES FOR CONCRETE.

Beam	(MPa)	(MPa)	(MPa)	υ
Control beam	1.930E+07	16708.75	2545.61	0.2
Flexure beam	1.758E+07	13744.98	2309.05	0.2
Shear beam	1.813E+07	14723.13	2389.58	0.2
Flexure-shear beam	1.758E+07	13744.97	2309.05	0.2

Stress-strain relationship for concrete in compression is important in FEM. It was obtained using expressions by Desayi and Krishnan [13] and was simplified as shown in Figure 9[14].

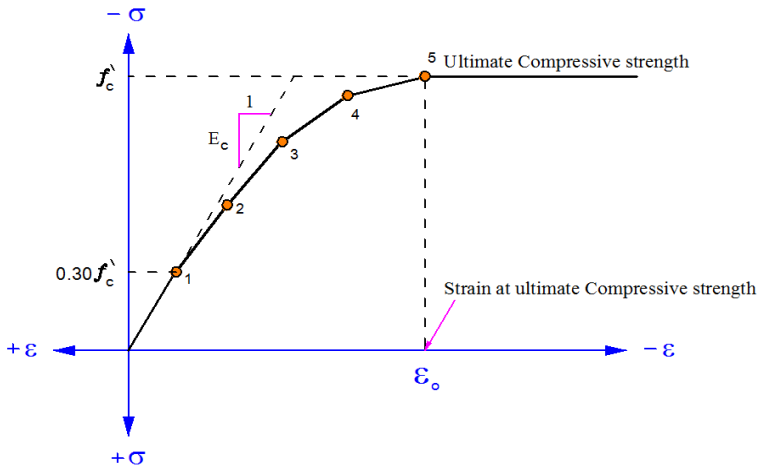

Figure 9: Simplified compressive uniaxial stress-strain curve for concrete.

3.2 Steel reinforcement and steel plates

The element LINK8 refers to all the steel reinforcement used in the beam. The properties of steel used in the model are the same as the experimental investigation by Kachlakev and McCurry [2]. The steel for the FEM was assumed to be bilinear isotropic. Material properties for the steel used in all models are shown in Table 2.

Element SOLID45 was used to model steel plates at support locations and loading points to avoid more stress concentration over the support areas and loading points. This element is modeled as a linear isotropic element as shown in Table 2.

Table 2: SUMMARY OF MATERIAL PROPERTIES VALUES FOR STEEL REINFORCED THE BEAM.

Properties	Steel reinforcement	Steel plate
	199948 (MPa)	199948 (MPa)
	413685 (MPa)	*
υ	0.3	0.3

* The stress strain curve of steel plate was considered as linear.

3.3 FRP Composites

FRP composites are composed of resins, reinforcements, fillers, and additives. Each of these constituent materials or ingredients plays an important role in the processing and final performance of the end product. FRP composites are anisotropic materials. FRPs were simulated as orthogonal material that has three planes *xy*, *xz*, and *yz*. The *xyz* coordinate axes are the principal coordinates for fibers. Local coordinate system is very important and is needed to define the FRP shell elements correctly. The *x* axis was in the same direction as the fiber direction.

The *y* axis was the direction of the width of the fiber while the *z* axis was perpendicular over the other axis. In this article, the FRP composites properties were chosen to be the same in both of *y* and *z* directions. A summary of material properties of FRP used for the modeling of all three beams is shown in Tables 3 and 4.

Table 3: SUMMARY OF MATERIAL PROPERTIES VALUES FOR CFRP.

FRP	Property	One layer	Two layers	Three layers
CFRP with thickness 1.016 mm	(MPa)	62053	124106	186158
	(MPa)	4826	9652	14478
	(MPa)	4826	9652	14478
		0.22	0.22	0.22
		0.22	0.22	0.22
		0.3	0.3	0.3
	(MPa)	3268	6536	9804
	(MPa)	3268	6536	9804
	(MPa)	1861	3722	5583

Table 4: SUMMARY OF MATERIAL PROPERTIES VALUES FOR GFRP.

FRP	Properties (psi)	Two layers	Four layers
GFRP with thickness 1.27 mm	(MPa)	41368	82737
	(MPa)	13789	27579
		13789	27579
		0.26	0.52
		0.26	0.52
		0.3	0.6
	(MPa)	3034	6068
	(MPa)	3034	6068
		5309	10618

3.4 Loading and boundary conditions

The locations of support and loading plates were considered the same as the full-size beams. The experimental steel plate dimensions for support were, and for loading. The steel plate was added to avoid stress concentration at the support and loading locations. The support was modeled as a roller support and hinged constraint at a one line of nodes under the plate in the *y*, and *z* directions. Also the load was applied vertically on center line of plate. Figure 10 illustrates the plate and applied loading.

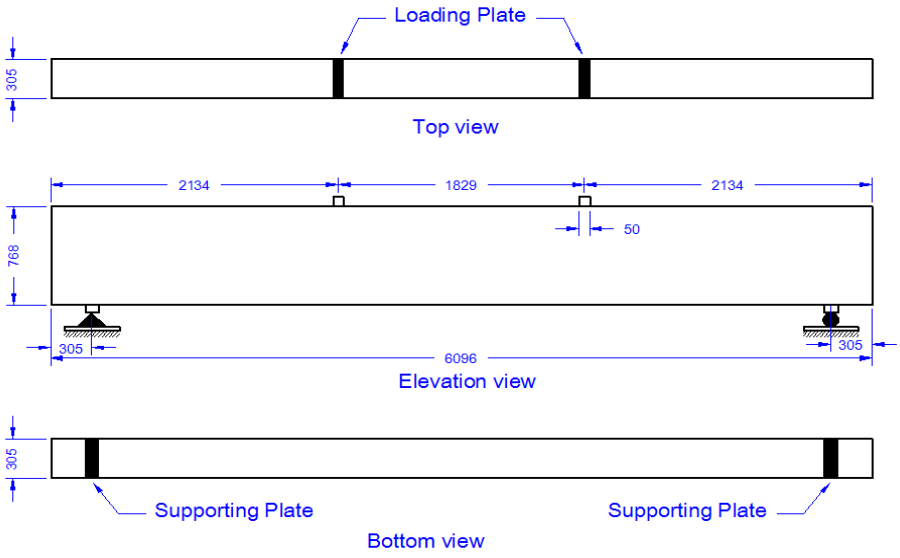

Figure 10: Loading and support locations (McCurry and. Kachlakev, 2000).

Due to symmetry conditions, a quarter of the beam is modeled. Symmetry constrains are applied at symmetry planes in the direction perpendicular to the plane of symmetry. At plane of symmetry parallel to *yz* plane, is equal to zero and at plane parallel to *xz*, is equal to zero.

3.5 Solution control and analysis of the model

In this research, static analysis is used for finite element model of simply supported beam under vertical loading. To preform solution at a specific range of load, load steps, sub steps and do loops were used. Data were recorded every load step to show all solution steps and to decrease the storage volume of recorded data. Sub steps option was used to control the conversion problem. Do-

loop option was used to control the conversion issue and to decrease the time required for solution. It should be noted that the time needed in the case of (Kachlakev and McCurry, 2001) [2] was around 120 hours to solve the model but with the current research this time was reduced to less than 1 hour.

4. Results from FEM of full-size beams

Results from the finite element analysis are compared with the experimental data for the full-size beams and with the theoretical results obtained by other researchers [1, 2]. The following comparisons are made:

- Load-strain plots at selected locations,
- Load-deflection plots at mid-span,
- First cracking loads, loads at failure and crack patterns at failure.

The data obtained from the theoretical analysis are at the same location of strain gauges used in experimental tests as shown in Figure 11.

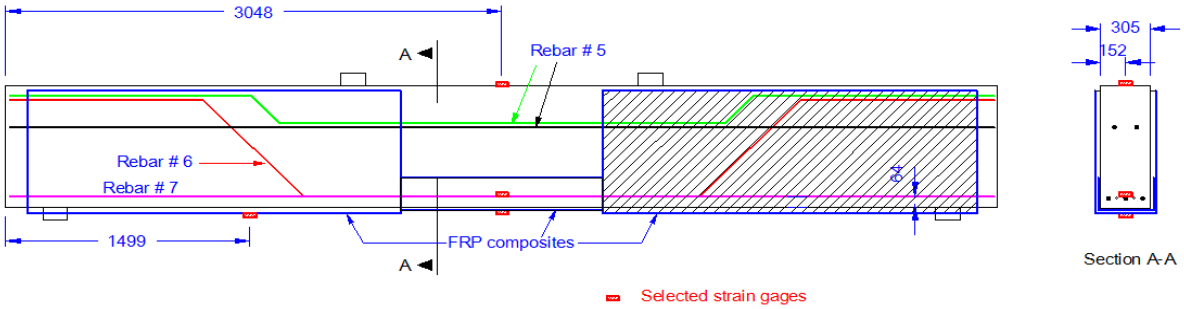

Figure 11: Selected strain gauge locations.

4.1 Load-Strain Plots

4.1.1 Tensile strain in lower steel reinforcing

From experimental beams strain data were collected using strain gauges fixed on steel bar # 7 at the mid-span the beams. The comparison between the total load and strain on bar #7 from finite element analysis and the experimental work are shown in Figures 12 and 13.

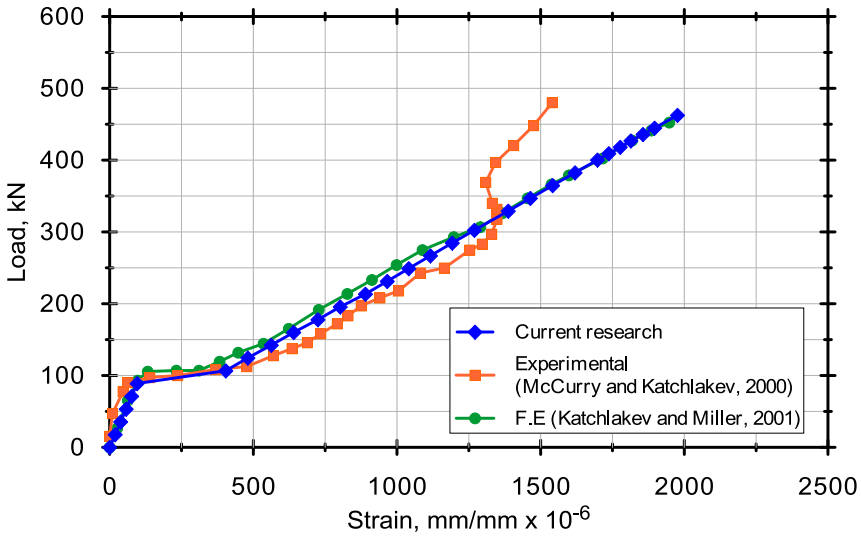

Figure 12: Load-strain curve for steel bar # 7 in the control beam.

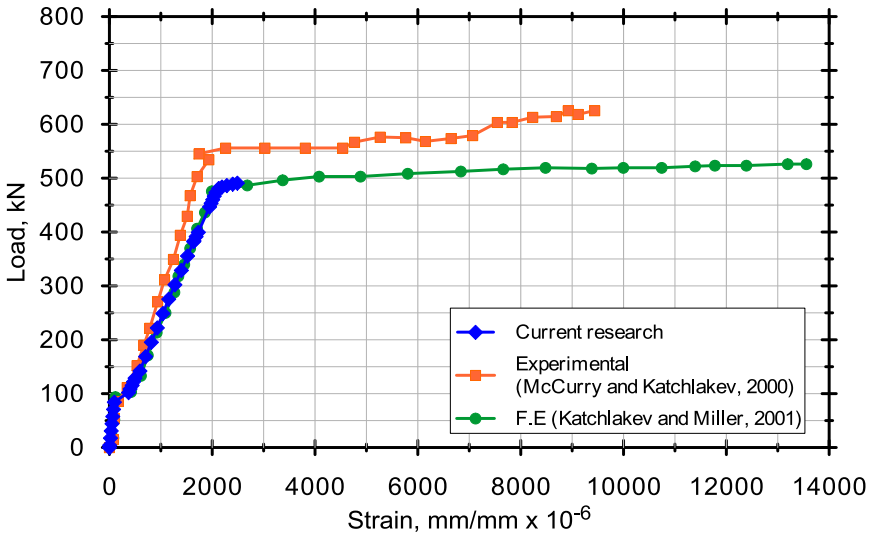

Figure 13: Load-strain curve for steel bar # 7 in shear beam.

It can be seen from these figures that the relationship between load and strain for main steel in current research was in good agreement with experimental results and theoretical results [1, 2] in linear strain portion and little difference in the nonlinear portion. In the experimental beams, concrete at the first crack can resist amount of tension but in the finite element model the stiffness decrease to zero, therefore the tension in steel element does not change as in experimental beams. Strains from FE were higher than experimental results done by (McCurry and Kachlakev, 2000) [2].

4.1.2 Compressive Strain in Concrete

Strain gauge was placed at mid-span on the top face for beams as shown in Figure 14. Comparison was made between the experimental results and FE analysis of previous research and current research for four beams tested and shown in Figures 14 and 15. Compressive strain curves for concrete have some difference between the experimental results and finite element result. This may be attributed to an experimental error in calibration or a defect in fixing the strain gages or a defect in the material of the concrete beams.

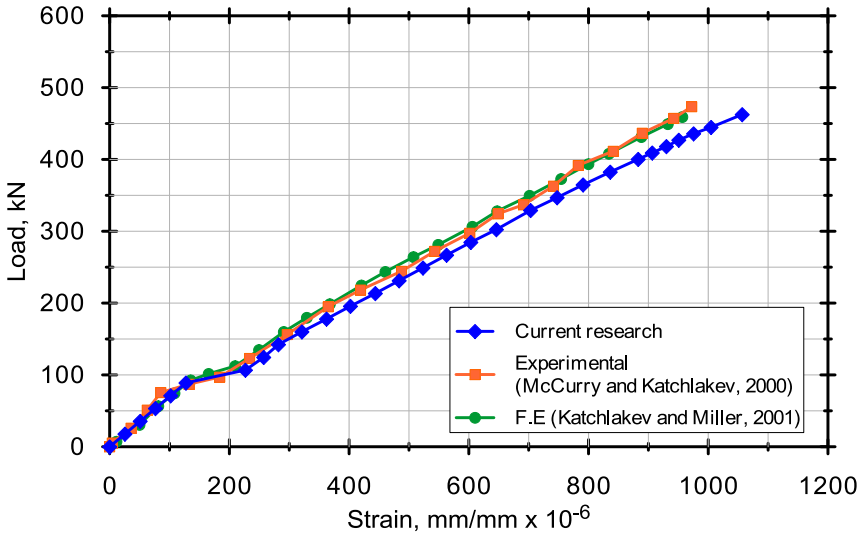

Figure 14: Load-compressive strain curve for concrete in control beam.

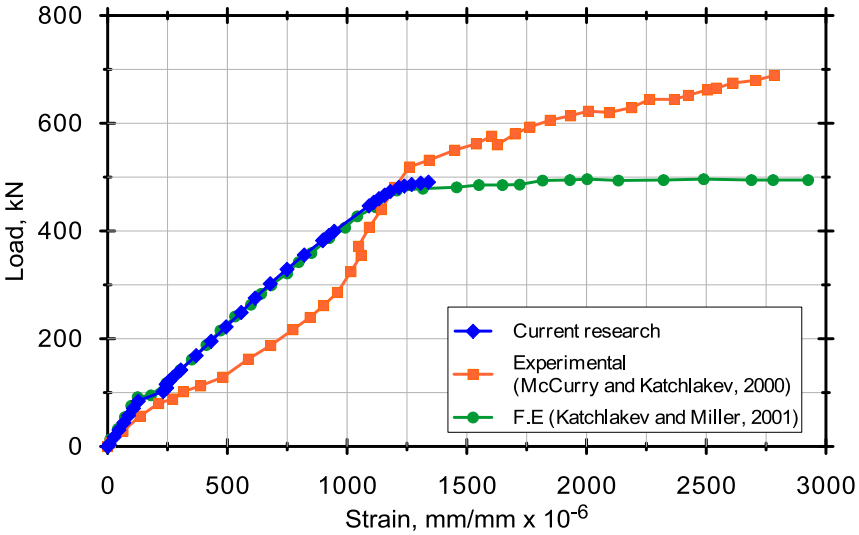

Figure 15: Load-compressive strain curve for concrete in shear beam.

4.1.3 Tensile Strain in FRP Composites

Strains in FRP composites were measured at the bottom of the beam at mid-span on the surface of the CFRP composite as shown Figure 11. For the shear beam the strain was collected from the bottom of the beam at far from the end of the beam. Comparisons of the total load on the beam with strain in FRP collected from experimental results and previous FE analysis and current research are shown from Figures 16 and 17. Also the strain obtained from the current research in GFRP for shear beam gets good agreement with experimental and better results than those of the FE by Kachlakev and Miller, 2001.

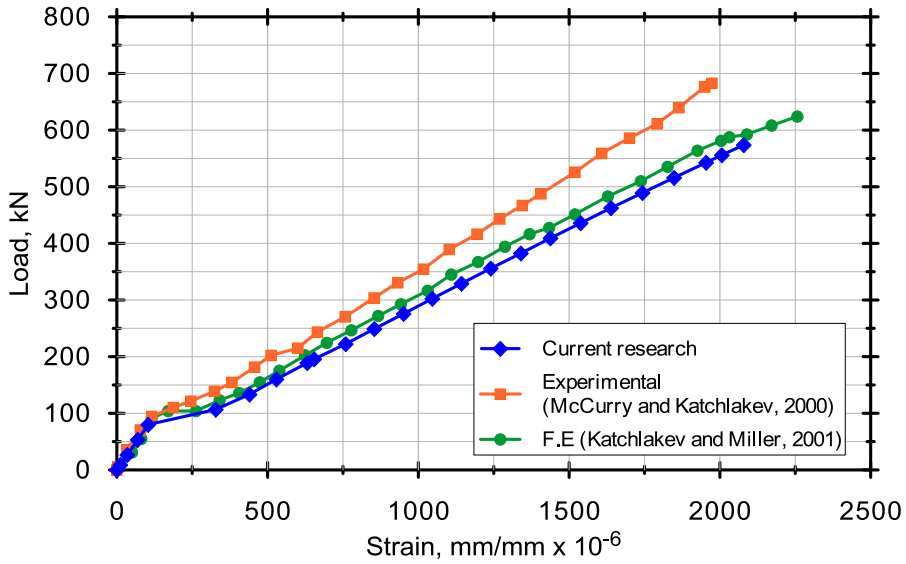

Figure 16: Load strain curve in the CFRP for the flexure beam.

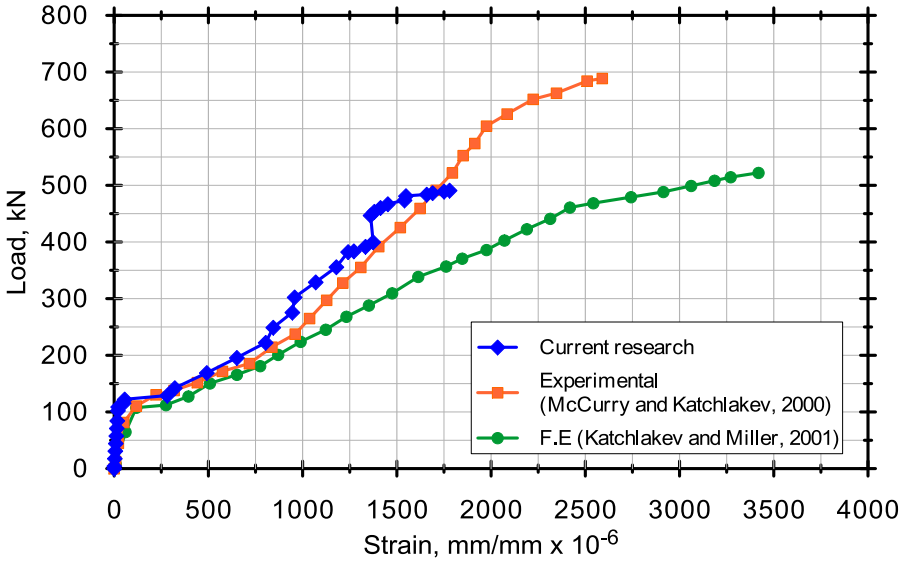

Figure 17: Load strain curve in the GFRP for the shear beam.

4.1.4 Load-Deflection Relationship

The deflection was measured at mid-span of each beam. The deflection data collected from FE in the current study was measured at the same location of the experimental beam. The comparison for load deflection curve obtained from experimental results and previous analytical research and current research using FE are shown in Figures 18 to 19. The load deflection relationship indicates good agreement between experimental results and the finite element results with some deviation. The factors that can lead to this difference are micro cracks formed during drying and the full bond assumption in the finite element model. The micro cracks reduce the stiffens of the tested beams and the full bond between steel and concrete in finite element model add some stiffness as there is no slip between the bars and the concrete during the nonlinear behavior.

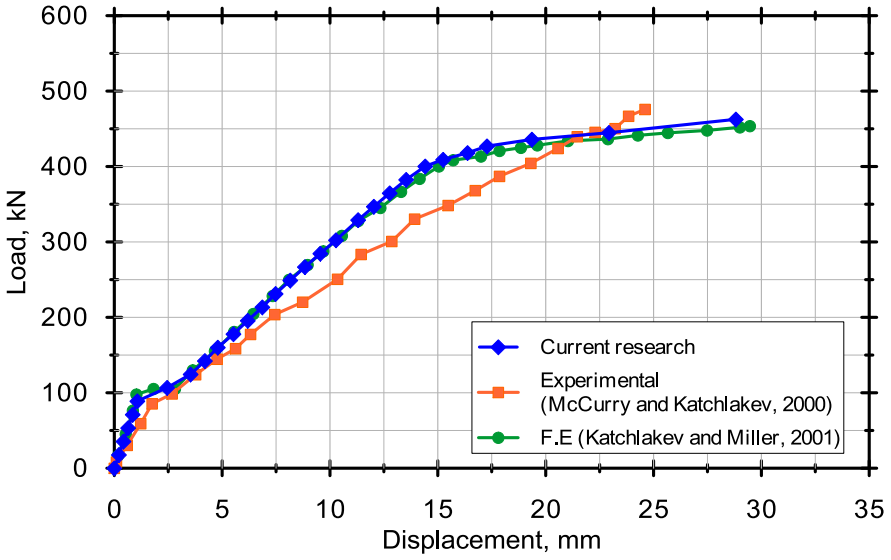

Figure 18: Load-displacement curve for control beam.

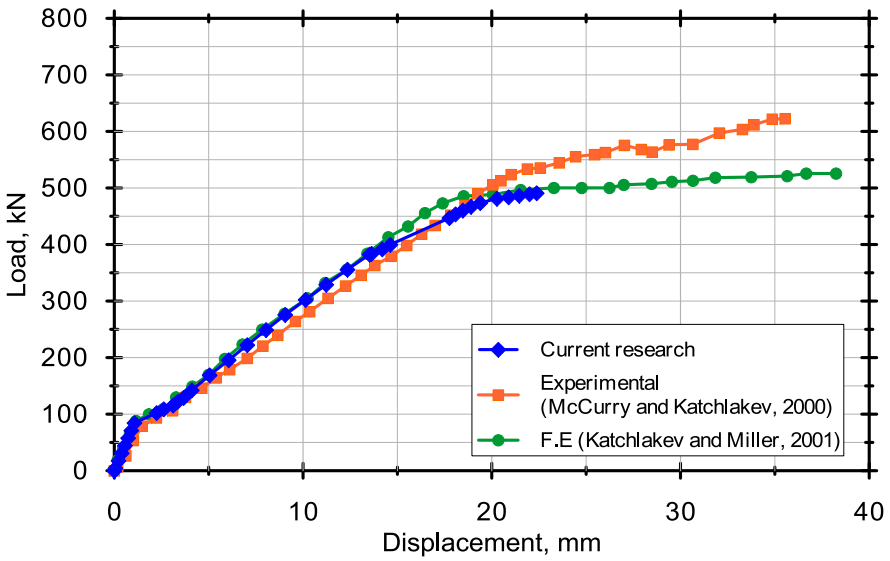

Figure 19: Load-displacement curve for shear beam.

Figure 20 shows the load deflection relationship between the beams solved by FE. The curves indicated that in the linear part the stiffness of beams for control beams and strengthened beams are the almost same. But after the linear zone, the beams strengthened with FRP get high stiffness than the control beams. The strengthened beams are capable of carrying higher loads.

4.1.5 Crack Patterns for the Studied Beams

ANSYS permits to see the crack pattern in different load steps until failure. The crack appears when the tensile stress reaches the ultimate stress. The cracks are drawn as small circles and take direction perpendicular to the direction of the principle stress. The crack pattern is shown in Figures 21 to 22.

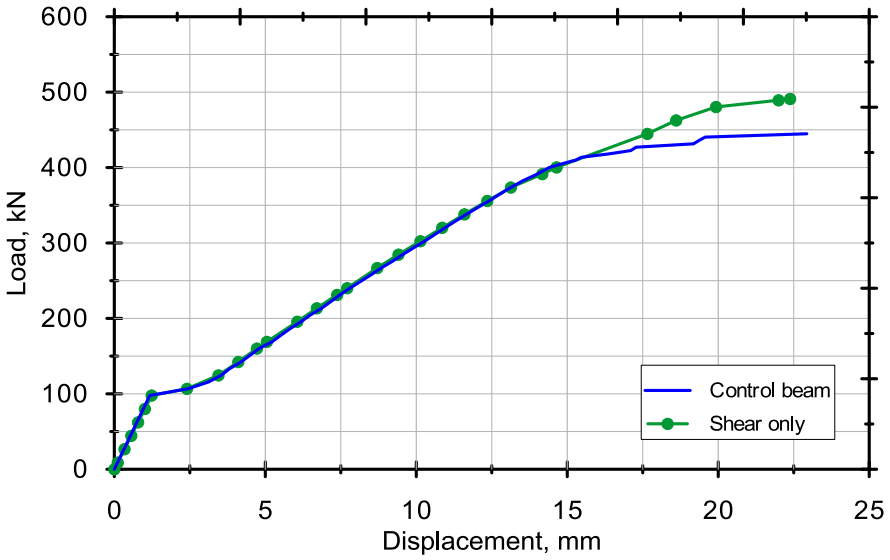

Figure 20: Load-displacement curves for the studied beams solved by FEM.

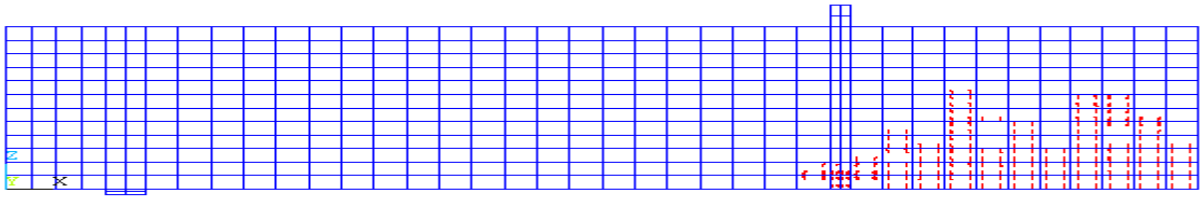

(a)

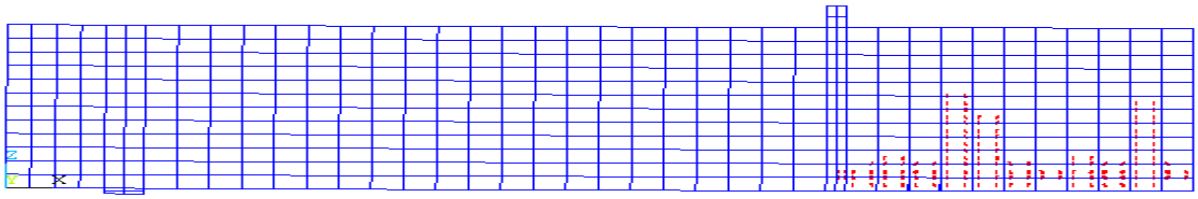

(b)

Figure 21: (a) crack pattern for control beam at first crack (24 kips)
(b) Crack pattern for shear strengthening beam at first crack (22.5 kips)

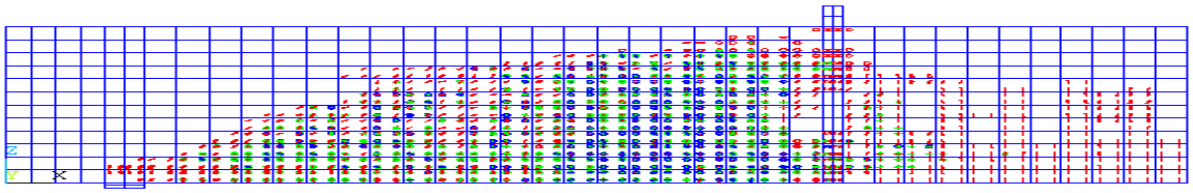

(a)

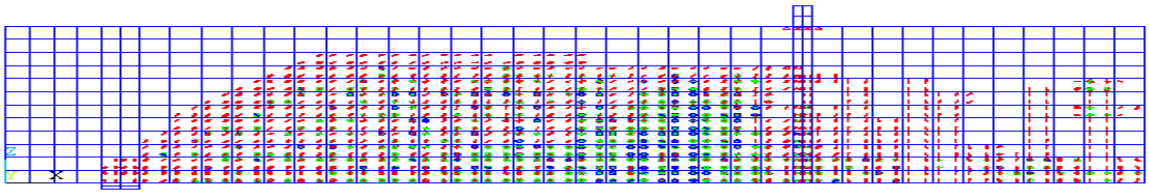

(b)

Figure 22: (a) crack pattern for control beam at load 104 kips
(b) Crack pattern for shear strengthening beam at load 110 kips

5. Conclusion and recommendations

This research presented an efficient FEM to predict the behavior of reinforced concrete beams strengthened with FRP. The presented model was able to solve the nonlinear behavior of concrete beams with and without FRP reinforcement in a very short time compared to other previous models. Results from FE model and experimental work were compared and presented.

The model showed good agreement with previous FE models and experimental work. Real beams were studied to simulate the beams used in Horsetail Creek Bridge in Oregon, USA. Results were presented in the form of load-strain plots for concrete, steel and fiber. In addition, the load deflection curves and crack patterns were also represented.

The results showed that the modeling process was accurate in simulating the tested beams. It was also shown that using FRP in strengthening reinforced concrete beams is an effective method. The following conclusions are drawn from this study:

- A comparison between the previous experimental and theoretical results with this research was performed. The results showed good agreement between previous researches and the current research.
- The current model proofed to be a good technique that can be used to produce acceptable theoretical results with ease in application.
- Using shell elements is more accurate in simulating the FRP composites.
- From the current results it was clear that strengthening of beams in shear using strips of fiber or with continuous sheets did not show much difference.
- A subroutine was to model the concrete beams reinforced with FRP which gave a better control in modeling and run of the problem. This led to tremendous time saving from 120 hours to less than one hour having the same or better results.

REFERENCES:

[1] Abdel-Jaber, M.S., Walker, P.R., and Hutchinson, A.R. (2003), Shear Strengthening of reinforced concrete beams using different configurations of externally boned carbon fiber reinforced plate. Materials and Structures, Vol. 36, pp 291-301.

[2] Kachlakev, D., and McCurry, D.D., (2000), "Behavior of full-scale reinforced concrete beams retrofitted for shear and flexural with FRP laminates," Composites: Part B, 31, pp. 445-452.

[3] Chajes, M.J., Thomson, T.A., Farschman, J.A., and Farschman, C.A., (1995), "Durability of concrete beams externally reinforced with composite fabrics," Construction and Building Materials, Vol. 9, No. 3, pp. 141-148.

[4] Gao, B., Kim, J.-K., and Leung, C.K.Y., (2004), "Experimental study on RC beams with FRP strips bonded with rubber modified resins," Composites Science and Technology, 64, pp. 2557–2564.

[5] Toutanji, H., and Ortiz, G., (2001), "The effect of surface preparation on the bond interface between FRP sheets and concrete members," Composite Structures, 53, pp. 457-462.

[6] Obaidat, Y.T., Heyden, S., and Dahlblom, O., (2010), "The effect of CFRP and CFRP/concrete interface models when modeling retrofitted RC beams with FEM," Composite Structures, 92, pp. 1391–1398.

[7] Yang, Z.J., Chen, J.F., and Proverbs, D., (2003), "Finite element modelling of concrete cover failure in FRP plated RC beams," Construction and Building Materials, 17, pp. 3–13.

[8] Hawileh, R.A., Naser, M., Zaidan, W., and Rasheed, H.A., (2009), "Modeling of insulated CFRP-strengthened reinforced concrete T-beam exposed to fire," Engineering Structures, 31, pp. 3072-3079.

[9] Aram, M.R., Czaderski, C., and Motavalli, M., (2008), "Debonding failure modes of flexural FRP-strengthened RC beams," Composites: Part B, 39, pp. 826–841.

[10] Chen, J.F., Yuanb, H., and Tengc, J.G., (2007), "Debonding failure along a softening FRP-to-concrete interface between two adjacent cracks in concrete members," Engineering

Structures, 29, pp. 259–270.

[11] Yao, J., and Teng, J.G., (2007), "Plate end debonding in FRP-plated RC beams—I: Experiments," Engineering Structures, 29, pp. 2457–2471.

[12] Perera, R., Barchín, M., Arteaga, A., and De Diego, A., (2010), "Prediction of the ultimate strength of reinforced concrete beams FRP-strengthening shear using neural networks," Composites: Part B, 41, pp. 287–298.

[13] Desayi, P. and Krishnan, S. (1964). Equation for the stress-strain curve of concrete, ACI Journal, Proc. 61(3):345-350.

[14] Kachlakev, D., Miller, T., Yim, S., Chansawat, K. and Potisuk, T. (2001). "Finite Element Modeling of Concrete Structures Strengthened with FRP Laminates," Final Report, SPR 316, Report No. FHWA-OR-RD-01-17, for Oregon Department of Transportation, Salem, OR, and Federal Highway Administration, Washington, DC, May 2001, 111 pp.